One-dimensional topological superconductivity based entirely on phase control

Omri Lesser⊙, Yuval Oreg, and Ady Stern
Department of Condensed Matter Physics, Weizmann Institute of Science, Rehovot 7610001, Israel

Topological superconductivity in one dimension requires time-reversal symmetry breaking, but at the same time, it is hindered by external magnetic fields. We offer a general prescription for inducing topological superconductivity in planar superconductor-normal-superconductor-normal-superconductor (SNSNS) Josephson junctions without applying any magnetic fields on the junctions. Our platform relies on two key ingredients: the three parallel superconductors form two superconductor-normal-superconductor junctions with phase winding, and the Fermi velocities for the two spin branches transverse to the junction must be different from one another. The two phase differences among the three superconductors define a parameter plane which includes large topological regions. We analytically derive the critical curves where the topological phase transitions occur and corroborate the result with a numerical calculation based on a tight-binding model. We further propose material platforms with unequal Fermi velocities, establishing the experimental feasibility of our approach.

Introduction. Topological superconductivity is a novel phase of matter with fascinating edge physics [1–4]. In one dimension (1D), topological superconductors host Majorana zero modes at their ends, which possess exotic exchange properties [5]. In experimental setups, attempts to engineer topological superconductors rely on proximity-coupling to nontopological *s*-wave superconductors and employing strong spin-orbit coupling (SOC) to separate the two spin species. Furthermore, time-reversal symmetry has to be broken to lift the Kramers degeneracy. When judiciously combined, these three ingredients—conventional superconductivity, a spin-rotation mechanism and time-reversal symmetry breaking—make the low-lying energy band effectively spinless whereas maintaining superconducting pairing, thus, giving rise to spinless topological superconductivity.

Much effort has been devoted to inducing topological superconductivity in various experimental platforms [6,7]. One of the first proposals [8] utilized the surface of topological insulators [9,10] in proximity to a superconductor. Other prominent proposed Majorana platforms include semiconductor-ferromagnet heterostructures [11], quantum wells with an in-plane magnetic field [12], and chains of magnetic adatoms on superconductors [13,14]. Early on, semiconductor-superconductor nanowires were put forward as an accessible platform [15,16]. Nanowires have since then been vigorously studied: Theoretical extensions of the original models were made to include current biasing [17], disorder [18,19], electrostatics [20], full-shell nanowires [21,22], as well as electron-electron interactions [23–25]. On the experimental side, several groups have reported possible signatures of Majorana zero modes in proximitized nanowires [22,26–31], but they are not entirely definitive [18,32,33].

The experimental drawbacks of the nanowire platform is the need for large magnetic fields, which hinder superconductivity and create unwanted subgap states [34,35], and the sensitivity to the chemical potential, which requires delicate gating [36]. An important advancement came in the form of planar phase-biased Josephson junctions [37–40] [also known as superconductor-normal-superconductor or (SNS) junctions]. There, time-reversal symmetry is broken by both an in-plane Zeeman field and a superconducting phase bias, which define a two-dimensional parameter plane. Large regions of this parameter plane are topological, including, in principle, regions with weak magnetic fields. In the wire geometry, one typically assumes that the level spacing between the transverse modes d is larger than the induced superconducting gap Δ. In contrast, in the planar geometry $d \ll \Delta$ so that many modes participate in the formation of the topological state, and, therefore, the boundaries of the topological regions depend only weakly on the system's chemical potential [38,41]. Several experimental results indeed show the potential and versatility of this platform [42–46]. However, to get an appreciable topological gap, one still needs to apply significant magnetic fields.

Our goal in this paper is to induce topological superconductivity in a planar system, using only phase biasing and without applying any Zeeman field. First steps in this direction were previously taken [8,47–51] (for a recent review see Ref. [52]). Here we provide a straightforward recipe based on simple principles which are sufficient to achieve this goal and propose materials suitable for realizing our recipe.

Two key points allow us to accomplish this objective. The first is the introduction of two phase differences by including three superconductors in our system. With these two phase differences, we show that phase winding can drive the system into a topological phase. The second pivotal element is unequal Fermi velocities for the two spin branches in the direction transverse to the junction. The combination of these two ingredients can replace the external Zeeman field altogether.
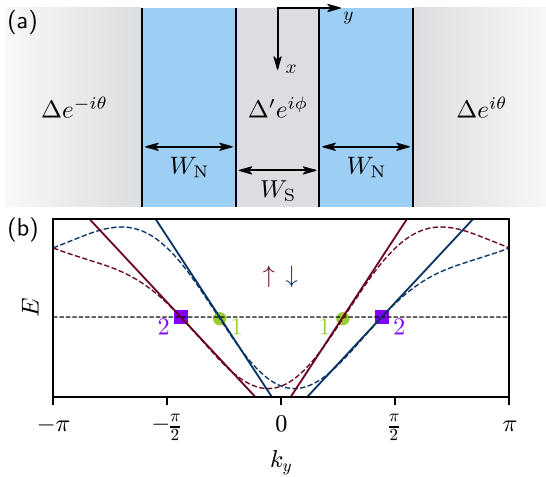
FIG. 1. (a) Phase-biased superconductor-normal-superconductor normal-superconductor (SNSNS) junction (superconducting regions are gray and normal regions are blue). The two outer superconductors are semi-infinite in the transverse direction y, and their superconducting order parameter Δ is, in general, different than the one of the middle superconductor Δ'. At $k_x = 0$ this reduces to a one-dimensional problem, whose zero-energy crossings correspond to topological phase transitions. (b) Transverse spectrum of the junction (dashed lines) in a model including next-nearest-neighbor hopping (see the Supplemental Material [53]). At the Fermi energy (dashed black line), there are four Fermi points. The Fermi velocities at the "outer" branch (purple squares) and in the "inner" branch (green dots) are not identical. Solid lines correspond to the linearized spectra.

Phase winding and unequal Fermi velocities. In one-dimensional superconducting systems where time-reversal symmetry is broken and translational invariance holds, a transition between trivial and topological phases occurs when there is a single gap closing at zero longitudinal momentum ($k_x = 0$). For a single Josephson junction, the closure of the gap happens when a single pair of eigenstates of the Bogoliubov–de Gennes Hamiltonian crosses zero energy [5] as we tune the phase bias across the junction. Evidently, for such a single gap closing to occur, spin symmetry must be broken. Indeed, the application of the Zeeman field separates between the gap closing curves of the two spin branches in the parameter space, thereby, separating trivial and topological regions [37,38]. We now show that when the two branches have different velocities, and the single Josephson junction is replaced by two junctions in series, the Zeeman field may be replaced by a second phase difference.

We first consider a SNS junction between two superconductors whose order parameters are $\Delta e^{\pm i\theta}$. If the superconducting gap Δ is much smaller than the Fermi energy E_F, then, at $\theta = \pi/2$ where the phase difference across the junction is π, a double gap closing occurs, with four states at zero energy. Starting from this point, we introduce a third superconductor in the middle of the junction with an order parameter $\Delta' e^{i\phi}$, see Fig. 1(a), and search for single gap-closing curves in θ-ϕ space. The regions between such curves are topological.

To this end, we construct a simple model describing a SNSNS geometry with two linearly dispersing branches
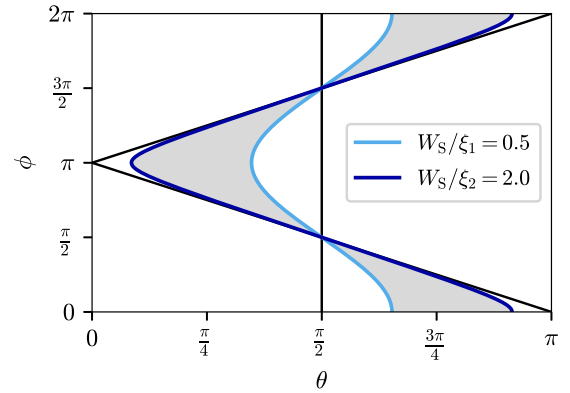

FIG. 2. Phase diagram for the SNSNS geometry of Fig. 1, derived from Eq. (1). The two values $\xi_j = v_j/\Delta'$ originate from the unequal transverse Fermi velocities $v_1 \neq v_2$. The light and dark blue curves correspond to zero-energy crossings at $k_x = 0$ for $W_S/\xi_1 = 0.5$ and $W_S/\xi_2 = 2$, respectively. Since each of these crossings is nondegenerate, it corresponds to a topological phase transition, and, therefore, the area between the curves (shaded) harbors a topological superconducting state. The black lines define the region where a vortex is present.

$j = 1, 2$ with the normal-state Hamiltonian $H_{0,j}^{\pm} = \pm i v_j \partial_y$ where the $\pm$ indicates the two opposite directions of motion across the junction, see Fig. 1(b), and we set $\hbar = 1$ (a similar system was studied in Refs. [54,55]). As we study below, under certain conditions, spin-orbit coupling may make the velocities v_1, v_2 unequal, which will be important in what follows. At $k_x = 0$, this two-dimensional (2D) system along the y direction becomes effectively one dimensional, and finding the bound states involves a standard calculation whose details are given in Sec. SI of the Supplemental Material [53]. We find that for the jth branch there is a single gap closing along a line on the θ-ϕ plane defined by

$$\cos\theta + \tanh\left(\frac{W_S \Delta'}{v_j}\right)\cos\phi = 0, \qquad (1)$$

where W_S is the width of the middle superconductor.

Several aspects of Eq. (1) are noteworthy. First, we see that the position of the gap-closing transition within the θ-ϕ plane is determined by the dimensionless ratio W_S/ξ_j, where $\xi_j = v_j/\Delta'$ is the coherence length of the middle superconductor for branch j. When the middle superconductor is absent ($W_S = 0$), the transition occurs for both branches at $\theta = \pi/2 + \pi n$ (here n is an integer). When the middle superconductor is very wide, the system may be seen as two disconnected junctions, and a gap closing takes place when the phase difference across *one* junction is $\phi \pm \theta = \pi + 2\pi n$. In between, the position of the gap closing creates a curve on the θ-ϕ plane. When the velocities in the middle superconductor v_1, v_2 are unequal, the gap-closing curves for the two branches are different [see Eq. (1)], and constitute topological class D phase transitions. The topological region they define is maximized when, without loss of generality, $\xi_1 \ll W_S$ and $\xi_2 \gg W_S$ (see Fig. 2, and the discussion in Sec. SIII of the Supplemental Material [53]). Interestingly, as we show in Sec. SI of the Supplemental Material [53], Eq. (1), which determines the phase boundaries, is independent of the width

and velocities of the normal regions. This independence has important practical consequences since, generally, a narrow normal part leads to a relatively large gap for the Andreev states away from the transitions. In previous proposals [37,38,56], other considerations did not allow for arbitrarily narrow normal parts.

Although our analysis assumed the absence of disorder, the emerging picture suggests a qualitative criterion for its effect. As we saw, in order to obtain a well-separated single gap closing, one branch should traverse the entire middle superconductor, whereas the other should be reflected back from that superconductor. To this end, it is required that disorder will be weak enough such that no significant interbranch scattering would occur on a scale of W_S. The absence of a Zeeman field should increase the robustness of our platform to potential impurities, which will not hinder the proximity effect as in existing Majorana platforms. In addition, we require that smooth potential fluctuations are sufficiently weak to keep the velocities unequal. We also find in Sec. SVIII of the Supplemental Material [53] that nonperfect normal-superconductor interfaces do not alter the picture significantly.

Our analysis, which focused on the case of two branches, may easily be generalized to situations where there are more branches. This could happen, for example, due to having more than one subband in the z direction or due to having more than two bands with states at the Fermi energy. With many branches there would be many single-gap closings, and, therefore, many transitions between trivial and topological regions on the θ-ϕ plane. A well-separated single-gap closing requires a Fermi velocity that is significantly different from the other Fermi velocities.

Remarkably, for all values of W_S/ξ the curves defined by Eq. (1) and the topological regions they induce correspond to phase configurations in which the phase winds by 2π (in agreement with Ref. [57]). As shown previously [50], a 2π-phase winding occurs when $g = (\cos\theta + \cos\phi)\cos\theta < 0$ (see the Supplemental Material [53]). By Eq. (1),

$$g = -\tanh\left(\frac{W_S}{\xi_j}\right)\left[1 - \tanh\left(\frac{W_S}{\xi_j}\right)\right]\cos^2\phi. \quad (2)$$

Since $0 < \tanh(W_S/\xi_j) < 1$, Eq. (2) always implies a phase winding.

Obtaining unequal Fermi velocities for the two spin branches. Following the above observations, we now turn to search for setups in which the Fermi velocities for the two spin branches are unequal. We begin by discussing several material platforms where the band structure naturally has such an imbalance and continue by discussing how it may be artificially created.

Monolayers of transition-metal dichalcogenides (TMDs) [58–63] constitute a platform that is particularly suitable for our purposes, for two reasons. First, due to the strong spin-orbit coupling in TMDs, it is quite easy to find directions along which the Fermi velocities distinguish between the spin branches. In TaS$_2$, for example, we found a velocity imbalance as large as $v_</v_> = 0.7$ using an effective six-band Hamiltonian [64] (here $v_>$ is the larger velocity of the two, and $v_<$ is the smaller one). Moreover, we used a well-studied six-band tight-binding model [65] of MX_2

($M = $ Mo, W; $X = $ S, Se, Te) to show that these TMDs also support similar velocity imbalances.

Second, the SOC in the TMDs is of the Ising type in which the spins are polarized in the out-of-plane direction with the sign of polarization depending on the momentum. This property endows TMDs their giant critical field in the superconducting state, but it also makes them unsuitable for the setups of Refs. [37,38] where the SOC suppresses the spins' sensitivity to a Zeeman field. Since our scheme makes no use of a Zeeman field, this difficulty is alleviated. The remarkable combination of intrinsic gate-controlled superconductivity and unequal Fermi velocities in monolayers of WTe$_2$, for example, could open the door to topological superconductivity in a single material system without the need to proximity couple it to an external superconductor.

Beyond TMDs, calculations for quasi-one-dimensional wires defined by gates operating on HgTe quantum wells [66] show a similar velocity imbalance (see the Supplemental Material [53]). Given the velocity imbalance, our theory provides a practical guide to designing the device geometry to optimize the stability of the topological phase (see the Supplemental Material [53]).

Inducing unequal Fermi velocities: general considerations. To analyze possible sources for velocity imbalance, it is instructive to start from one-dimensional systems. In a 1D ring constrained to have only nearest-neighbor hopping, the most general spin-orbit coupling leads to the dispersion $E_\pm(k)$ of the two spin branches being rigidly shifted along the k axis, $E_\pm(k) = E(k \pm k_{SO})$ [67]. This may be understood by realizing that spin-orbit coupling introduces a spin-dependent Aharonov-Casher (AC) flux into the loop defined by the ring [68]. Then, the Fermi velocities (defined by $v_\pm = \partial E_\pm(k)/\partial k$) of the two spin branches are necessarily identical. The introduction of longer-range hopping, such as between next-nearest neighbors, expands the number of loops threaded by AC fluxes. Spin-orbit coupling then has a richer effect on the spectrum, which, in general, leads to unequal Fermi velocities.

As we now show, in two dimensions, nearest-neighbor hopping is sufficient to generate unequal Fermi velocities of the two branches when projected on to a certain direction The most general 2D band Hamiltonian of a monoatomic unit cell which is time-reversal symmetric and limited to nearest-neighbor hopping is

$$H_{2D}(\mathbf{k}) = -\sum_i t_i \cos(\mathbf{k} \cdot \mathbf{a}_i) - \sum_{i,\alpha} \lambda_\alpha^i \sin(\mathbf{k} \cdot \mathbf{a}_i)\sigma_\alpha, \quad (3)$$

where $\mathbf{a}_i$ ($i = 1, 2$) are the lattice's unit vectors, and $\alpha = x, y, z$ are Pauli matrix indices. We are interested in the dispersion and the velocities for $k_x = 0$. The x direction lies along the junction, and the orientations of the vectors $\mathbf{a}_i$ are left for tuning. If we choose the orientation of the lattice such that $a_{1,y}/a_{2,y} = n$, the 2D Hamiltonian $H_{2D}(k_x = 0, k_y)$ is identical to a 1D Hamiltonian with lattice constant $a_{1,y}$, and hopping amplitude to distances of $a_{1,y}$ and $na_{1,y}$, i.e., further neighbor hopping. For $n = 0, 1$, the problem maps onto the 1D ring with only nearest-neighbor coupling with identical Fermi velocities to both branches, whereas for $n \neq 0, 1$, the velocities are generically unequal. This mapping may easily
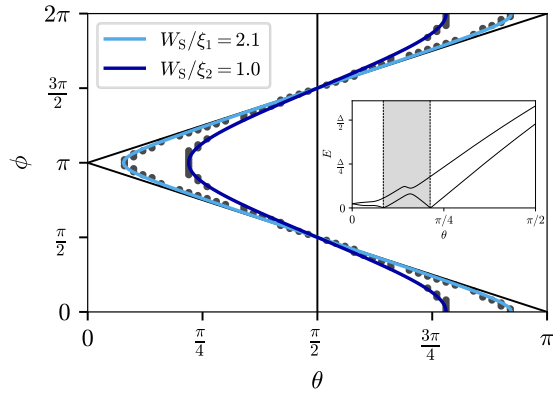
FIG. 3. Tight-binding simulation of the SNSNS junction of Fig. 1 at $k_x = 0$, showing the phase diagram as a function of the two phases θ and ϕ. The gray dots are the locations of the zero-energy crossings as calculated by the tight-binding simulation. The light and dark blue curves are fits of these points according to the analytical formula Eq. (1). We observe good agreement between the formula and the simulation (cf. Fig. 2), which also enables us to extract the two effective coherence lengths ξ_1, ξ_2. The inset: bound-state spectrum as a function of θ, the phase of the middle superconductor for $\phi = \pi$. The zero-energy crossings split along θ, rather than being degenerate. The resulting topological region is marked in gray. The simulation was performed according to Eq. (3) with the parameters $t_1 = t_2 = 1$, $\lambda_{1,y} = \lambda_{2,x} = 1.2$ (all other $\lambda_{i,\alpha} = 0$'s), $\mu = 3$, $\Delta = \Delta' = 0.1$, $W_N = 0$, $W_S = 80$. The left and right superconductors are each 200 sites wide.

be generalized to the case $a_{1,y}/a_{2,y} = n/m$ (with integers m, n and $m > 0$) and to 2D Hamiltonians that include long-range hopping amplitudes. Tight-binding calculations supporting this analysis are shown in Fig. 3.

We note, however, that for the angle dependence of the velocity to be manifest, we typically need to go beyond the second-order-in-k expansion of Eq. (3). At that order, the band structure for each angle is parabolic, and spin-orbit coupling results in a mere rigid shift of the parabolas. The parabolic approximation ceases to hold at large electronic densities, i.e., interelectron distance that is comparable to the lattice constant. Such densities are uncommon in semiconducting heterostructure-based two-dimensional electronic systems. Two different mechanisms may lead to unequal Fermi velocities of the two spin branches even at low densities. The first requires more than one subband in the z direction of the 2D electron gas with spin-orbit coupling strength depending on z [50], and the second requires a periodic potential [51].

The first mechanism may be understood by considering a heterostructure defined by a confining potential $V(z)$. In the absence of spin-orbit coupling, the confining potential defines spin-degenerate subbands in the z direction with the first two characterized by confinement energies 0, δE and by the real wave-functions $\chi_1(z)$, $\chi_2(z)$. The dispersion of each subband is quadratic. At low densities all higher subbands may be neglected, and we can project the spin-orbit coupling to the subspace defined by the two lowest subbands. Rashba SOC takes the form $H_R = \alpha(z)\mathbf{k} \times \boldsymbol{\sigma} \cdot \hat{z}$. Taking for simplicity $k_x = 0$ and projecting H_R to the subspace of the two lowest

subbands we get due to the spin, a 4×4 Hamiltonian,

$$H = \begin{pmatrix} \frac{k_y^2}{2m^*} & 0 \\ 0 & \frac{k_y^2}{2m^*} + \delta E \end{pmatrix} \sigma_0 + \begin{pmatrix} \alpha_{11} & \alpha_{12} \\ \alpha_{12} & \alpha_{22} \end{pmatrix} k_y \sigma_x, \quad (4)$$

in which m^* is the effective electron mass and $\alpha_{ij} \equiv \int dz\, \chi_i(z)\alpha(z)\chi_j(z)$. For z-independent α we have $\alpha_{12} = 0$. The subbands are then decoupled, and they are spin split to two shifted parabolas with equal velocities. When α depends on z the two subbands are coupled, and the velocities become unequal [69]. Details are given in Sec. SVII of the Supplemental Material [53].

A second mechanism for inducing unequal Fermi velocities is combining Rashba SOC with a periodic potential *along* the junction (in the x direction). A potential with wave-vector q mixes the states at $k_x = 0$, which do not experience SOC with states at $k_x = \pm q$ where SOC cannot be gauged away. Generically this leads to unequal Fermi velocities of the transverse modes. As a minimal model which demonstrates this possibility, we consider three superconducting pads deposited on top of a spin-orbit-coupled 2D electron gas. We apply a periodic modulation to the chemical potential of the middle superconductor $\mu(x) = \mu_0 + \delta\mu \cos(2\pi q x)$. Using a tight-binding discretization, we numerically calculate the spectrum and the topological invariant [70] for some integer values of q and find a topological phase transition (see Sec. SVI of the Supplemental Material [53]).

Outlook. Our work suggests a purely phase-controlled setup that induces topological superconductivity in an SNSNS devices, composed of two Josephson junctions in series. Our mechanism requires two conditions: superconducting phase winding and unequal Fermi velocities for the two electron branches. We find that the winding of the phase, which guarantees a net current flow through the two junctions, is a necessary condition for the topological state to form.

Unequal Fermi velocities in our setup are a consequence of spin-orbit coupling. We pointed out several examples of materials in which band-structure calculations predict unequal Fermi velocities for the two spin branches. Then, by studying microscopic models, we showed how unequal Fermi velocities may be generated at low densities, characteristic of semiconducting heterostructures. Remarkably, a common thread to the models we studied here, and those of earlier suggestions [50,51], is the essential role played by closed loops traversed by electrons and holes in which a spin-dependent Aharonov-Casher phase is accumulated. In the full-shell models [22,50], the closed trajectories are along the azimuthal cylinder direction; in the periodic potential case these are in-plane-closed orbits; and in the tight-binding model closed trajectories along a triangle in a basic unit cell will accumulate a nontrivial Aharonov-Casher phase. It seems that the combination of a discrete vortex in the three superconductors, superimposed with an Aharonov-Casher phase in closed trajectories leading to unequal Fermi velocities, is necessary to replace the Zeeman field in phase-only recipes for topological superconductivity.

The ubiquity of materials and engineered devices having unequal Fermi velocities makes our proposal within reach of current experiments. The elimination of any applied Zeeman

field should greatly aid in achieving reliable experimental results. Furthermore, the inherent periodicity of the phases will help distinguish the topological effect from trivial ones, and reliably map out the phase diagram (see Fig. S2 of the Supplemental Material [53]).

The code used for simulating the models and generating the plots in this Letter is available in Ref. [71].

[1] X.-L. Qi and S.-C. Zhang, Rev. Mod. Phys. **83**, 1057 (2011).

[2] J. Alicea, Rep. Prog. Phys. **75**, 076501 (2012).

[3] M. Leijnse and K. Flensberg, Semicond. Sci. Technol. **27**, 124003 (2012).

[4] B. A. Bernevig and T. L. Hughes, *Topological Insulators and Topological Superconductors* (Princeton University Press, Princeton, 2013).

[5] A. Y. Kitaev, Phys.-Usp. **44**, 131 (2001).

[6] R. M. Lutchyn, E. P. A. M. Bakkers, L. P. Kouwenhoven, P. Krogstrup, C. M. Marcus, and Y. Oreg, Nat. Rev. Mater. **3**, 52 (2018).

[7] K. Flensberg, F. von Oppen, and A. Stern, Nat. Rev. Mater. **6**, 944 (2021).

[8] L. Fu and C. L. Kane, Phys. Rev. Lett. **100**, 096407 (2008).

[9] M. Z. Hasan and C. L. Kane, Rev. Mod. Phys. **82**, 3045 (2010).

[10] J. K. Asbóth, L. Oroszlány, and A. Pályi, *A Short Course on Topological Insulators*, Lecture Notes in Physics Vol. 919 (Springer, Cham, 2016).

[11] J. D. Sau, R. M. Lutchyn, S. Tewari, and S. Das Sarma, Phys. Rev. Lett. **104**, 040502 (2010).

[12] J. Alicea, Phys. Rev. B **81**, 125318 (2010).

[13] F. Pientka, L. I. Glazman, and F. von Oppen, Phys. Rev. B **88**, 155420 (2013).

[14] S. Nadj-Perge, I. K. Drozdov, J. Li, H. Chen, S. Jeon, J. Seo, A. H. MacDonald, B. A. Bernevig, and A. Yazdani, Science **346**, 602 (2014).

[15] R. M. Lutchyn, J. D. Sau, and S. Das Sarma, Phys. Rev. Lett. **105**, 077001 (2010).

[16] Y. Oreg, G. Refael, and F. von Oppen, Phys. Rev. Lett. **105**, 177002 (2010).

[17] A. Romito, J. Alicea, G. Refael, and F. von Oppen, Phys. Rev. B **85**, 020502(R) (2012).

[18] H. Pan and S. Das Sarma, Phys. Rev. Res. **2**, 013377 (2020).

[19] H. Pan and S. Das Sarma, Phys. Rev. B **103**, 224505 (2021).

[20] S. D. Escribano, A. Levy Yeyati, Y. Oreg, and E. Prada, Phys. Rev. B **100**, 045301 (2019).

[21] T. D. Stanescu, A. Sitek, and A. Manolescu, Beilstein J. Nanotechnol. **9**, 1512 (2018).

[22] S. Vaitiekėnas, G. W. Winkler, B. van Heck, T. Karzig, M.-T. Deng, K. Flensberg, L. I. Glazman, C. Nayak, P. Krogstrup, R. M. Lutchyn, and C. M. Marcus, Science **367**, eaav3392 (2020).

[23] E. Sela, A. Altland, and A. Rosch, Phys. Rev. B **84**, 085114 (2011).

[24] E. M. Stoudenmire, J. Alicea, O. A. Starykh, and M. P. A. Fisher, Phys. Rev. B **84**, 014503 (2011).

[25] Y. Oreg, E. Sela, and A. Stern, Phys. Rev. B **89**, 115402 (2014).

[26] V. Mourik, K. Zuo, S. M. Frolov, S. R. Plissard, E. P. A. M. Bakkers, and L. P. Kouwenhoven, Science **336**, 1003 (2012).

[27] A. Das, Y. Ronen, Y. Most, Y. Oreg, M. Heiblum, and H. Shtrikman, Nat. Phys. **8**, 887 (2012).

[28] S. M. Albrecht, A. P. Higginbotham, M. Madsen, F. Kuemmeth, T. S. Jespersen, J. Nygård, P. Krogstrup, and C. M. Marcus, Nature **531**, 206 (2016).

[29] M. T. Deng, S. Vaitiekėnas, E. B. Hansen, J. Danon, M. Leijnse, K. Flensberg, J. Nygård, P. Krogstrup, and C. M. Marcus, Science **354**, 1557 (2016).

[30] A. Grivnin, E. Bor, M. Heiblum, Y. Oreg, and H. Shtrikman, Nat. Commun. **10**, 1940 (2019).

[31] S. Vaitiekėnas, Y. Liu, P. Krogstrup, and C. M. Marcus, Nat. Phys. **17**, 43 (2020).

[32] A. Vuik, B. Nijholt, A. Akhmerov, and M. Wimmer, SciPost Phys. **7**, 061 (2019).

[33] R. Hess, H. F. Legg, D. Loss, and J. Klinovaja, Phys. Rev. B **104**, 075405 (2021).

[34] D. Sabonis, O. Erlandsson, A. Kringhøj, B. van Heck, T. W. Larsen, I. Petkovic, P. Krogstrup, K. D. Petersson, and C. M. Marcus, Phys. Rev. Lett. **125**, 156804 (2020).

[35] M. Tinkham, *Introduction to Superconductivity*, 2nd ed., International Series in Pure and Applied Physics (McGraw-Hill, New York, 1996).

[36] A. C. Potter and P. A. Lee, Phys. Rev. B **83**, 094525 (2011).

[37] M. Hell, M. Leijnse, and K. Flensberg, Phys. Rev. Lett. **118**, 107701 (2017).

[38] F. Pientka, A. Keselman, E. Berg, A. Yacoby, A. Stern, and B. I. Halperin, Phys. Rev. X **7**, 021032 (2017).

[39] T. Laeven, B. Nijholt, M. Wimmer, and A. R. Akhmerov, Phys. Rev. Lett. **125**, 086802 (2020).

[40] P. P. Paudel, T. Cole, B. D. Woods, and T. D. Stanescu, Phys. Rev. B **104**, 155428 (2021).

[41] F. Setiawan, A. Stern, and E. Berg, Phys. Rev. B **99**, 220506(R) (2019).

[42] H. Ren, F. Pientka, S. Hart, A. T. Pierce, M. Kosowsky, L. Lunczer, R. Schlereth, B. Scharf, E. M. Hankiewicz, L. W. Molenkamp, B. I. Halperin, and A. Yacoby, Nature (London) **569**, 93 (2019).

[43] A. Fornieri, A. M. Whiticar, F. Setiawan, E. Portolés, A. C. C. Drachmann, A. Keselman, S. Gronin, C. Thomas, T. Wang, R. Kallaher, G. C. Gardner, E. Berg, M. J. Manfra, A. Stern, C. M. Marcus, and F. Nichele, Nature (London) **569**, 89 (2019).

[44] A. Banerjee, O. Lesser, M. A. Rahman, H.-R. Wang, M.-R. Li, A. Kringhøj, A. M. Whiticar, A. C. C. Drachmann, C. Thomas, T. Wang, M. J. Manfra, E. Berg, Y. Oreg, A. Stern, and C. M. Marcus, arXiv:2201.03453.

[45] A. Banerjee, O. Lesser, M. A. Rahman, C. Thomas, T. Wang, M. J. Manfra, E. Berg, Y. Oreg, A. Stern, and C. M. Marcus, arXiv:2205.09419.

[46] A. Banerjee, M. Geier, M. A. Rahman, D. S. Sanchez, C. Thomas, T. Wang, M. J. Manfra, K. Flensberg, and C. M. Marcus, arXiv:2205.15690.

[47] P. Kotetes, Phys. Rev. B **92**, 014514 (2015).

[48] R.-P. Riwar, M. Houzet, J. S. Meyer, and Y. V. Nazarov, Nat. Commun. **7**, 11167 (2016).

[49] A. Melo, S. Rubbert, and A. Akhmerov, SciPost Phys. **7**, 039 (2019).

[50] O. Lesser, K. Flensberg, F. von Oppen, and Y. Oreg, Phys. Rev. B **103**, L121116 (2021).

[51] O. Lesser, A. Saydjari, M. Wesson, A. Yacoby, and Y. Oreg, Proc. Natl. Acad. Sci. USA **118**, e2107377118 (2021).

[52] O. Lesser and Y. Oreg, J. Phys. D: Appl. Phys. **55**, 164001 (2022).

[53] See Supplemental Material at http://link.aps.org/supplemental/10.1103/PhysRevB.106.L241405 for details on the calculation of the bound-state energies in the SNSNS geometry at $k_x = 0$, a guide to choosing the parameters for optimal stability of the topological phase, a demonstration of obtaining a Fermi velocity mismatch from a simple tight-binding model with next-nearest neighbor hopping, a minimal model for topological superconductivity using a periodic potential applied along the junction, and a discussion of the effect of nonperfect normal-superconductor interfaces.

[54] M. Hurd and G. Wendin, Phys. Rev. B **51**, 3754 (1995).

[55] V. C. Y. Chang and C. S. Chu, Phys. Rev. B **55**, 6004 (1997).

[56] O. Lesser, G. Shavit, and Y. Oreg, Phys. Rev. Res. **2**, 023254 (2020).

[57] B. van Heck, S. Mi, and A. R. Akhmerov, Phys. Rev. B **90**, 155450 (2014).

[58] Q. H. Wang, K. Kalantar-Zadeh, A. Kis, J. N. Coleman, and M. S. Strano, Nat. Nanotechnol. **7**, 699 (2012).

[59] D. Xiao, G.-B. Liu, W. Feng, X. Xu, and W. Yao, Phys. Rev. Lett. **108**, 196802 (2012).

[60] X. Qian, J. Liu, L. Fu, and J. Li, Science **346**, 1344 (2014).

[61] S. Manzeli, D. Ovchinnikov, D. Pasquier, O. V. Yazyev, and A. Kis, Nat. Rev. Mater. **2**, 17033 (2017).

[62] S. Wu, V. Fatemi, Q. D. Gibson, K. Watanabe, T. Taniguchi, R. J. Cava, and P. Jarillo-Herrero, Science **359**, 76 (2018).

[63] K. Lee, T. Hazra, M. Randeria, and N. Trivedi, Phys. Rev. B **99**, 184514 (2019).

[64] G. Margalit, E. Berg, and Y. Oreg, Ann. Phys. (NY) **435**, 168561 (2021).

[65] G.-B. Liu, W.-Y. Shan, Y. Yao, W. Yao, and D. Xiao, Phys. Rev. B **88**, 085433 (2013).

[66] J. Reuther, J. Alicea, and A. Yacoby, Phys. Rev. X **3**, 031011 (2013).

[67] Y. Meir, Y. Gefen, and O. Entin-Wohlman, Phys. Rev. Lett. **63**, 798 (1989).

[68] Y. Aharonov and A. Casher, Phys. Rev. Lett. **53**, 319 (1984).

[69] L. Tosi, C. Metzger, M. F. Goffman, C. Urbina, H. Pothier, S. Park, A. L. Yeyati, J. Nygård, and P. Krogstrup, Phys. Rev. X **9**, 011010 (2019).

[70] M. Wimmer, ACM Trans. Math. Software **38**, 1 (2012).

[71] O. Lesser, Y. Oreg, and A. Stern, One-dimensional topological superconductivity based entirely on phase control, Zenodo, doi: 10.5281/zenodo.6645458 (2022).